Excited and Ionized States of *p*-Benzoquinone and Its Anion Radical: SAC−CI Theoretical Study

Yasushi Honda, Masahiko Hada, Masahiro Ehara, and Hiroshi Nakatsuji*

Department of Synthetic Chemistry and Biological Chemistry, Graduate School of Engineering, Kyoto University, Sakyo-ku, Kyoto 606-8501 Japan

Received: August 20, 2001; In Final Form: January 7, 2002

Excited and ionized states of *p*-benzoquinone (*p*-BQ) and the ground and excited states of its anion radical were studied by the SAC (symmetry adapted cluster)/SAC−CI (configuration interaction) method. Calculated ionization energies were in good agreement with the experimental ionization spectra, and the ionization peaks up to ca. 20 eV were assigned. The lowest four ionized states were calculated to be n_g^-, n_u^+, π_u^+, and π_g^+ in increasing energy order differently from the Koopmans' energy order, π_g^+, π_u^+, n_g^-, and n_u^+. The adiabatic electron affinity of *p*-BQ was calculated to be 1.96 eV in comparison with the experimental values, 1.86, 1.89, and 1.99 eV. The lowest allowed excitation of *p*-BQ anion radical was assigned to ^2A_u (π_g^{-}*$_{SOMO}$−π_u^{-}* shape resonance) for both the anion and neutral-state geometries. The assignment to $^2B_{3u}$ as the lowest allowed state by Tripathi et al. seems to be due to the exchange of the ^2A_u and $^2B_{3u}$ states by the hydrogen bonds with water solvent, which was supported by the SAC−CI calculations for *p*-benzosemiquinone (*p*-BQH) radical. With support from the proposal in the literature, two forbidden n−π*$_{SOMO}$ transitions were calculated below the lowest peak (^2A_u) for the anion geometry, whereas for the neutral geometry, these transitions were calculated to be less stable than the ^2A_u state. The two states observed above the ^2A_u state in various spectra were both assigned to $^2B_{3u}$ ($\pi_u^+-\pi_g^-$*$_{SOMO}$ and π_g^-*$_{SOMO}-\pi_u^+$*): the order of these states depends on the geometries, i.e., π_g^-*$_{SOMO}-\pi_u^+$* Feshbach resonance was lower in the anion geometry, whereas $\pi_u^+-\pi_g^-$*$_{SOMO}$ shape resonance was lower in the neutral geometry. The ordering is explained by the effect of geometry on the orbitals.

1. Introduction

Quinones are well-known as acceptors in the electron-transfer (ET) system, and their importance can be widely found in chemistry, biology, and industry. For example, they are found in biology as ubiquinone and menaquinone in the photosynthetic reaction center of *Rhodopseudomonas viridis*.[1,2] The route and the mechanism of the ET between these quinones were recently studied in our laboratory[2d] in a series of theoretical studies of photosynthetic bacteria.[2] They are also found in the active sites of anthracyclines that exhibit an antitumor activity.[3] Cigarette tar contains many different kinds of free radicals, and a predominant species is said to be a complex of quinone and hydroquinone groups.[4] In industry, quinones are used as oxidants and synthetic dyes. They work as acceptors in many CT-type organic conductors,[5] and in particular, quinhydrone (hydroquinone-benzoquinone complex) crystal[6] is well-known and used as an electrode. Among quinones, *p*-benzoquinone (*p*-BQ) is a key compound and, therefore, is important as a reference molecule in studying the electronic structures and functions of quinone species. In particular, the investigations of the electronic structures of the neutral *p*-BQ and its anion radical are necessary for understanding the nature of the electron-transfer systems including quinones.

Many experimental and theoretical studies have been reported on the electronic structure of *p*-BQ. Experimental studies on the singlet electronic excited states have been reported in gas phases,[7] in *n*-hexane,[8] and in crystals.[7a,9] Most of the theoretical studies were those using the semiempirical method,[7a,10] though several ab initio calculations have also been reported.[11] It is established both experimentally and theoretically that the lowest four singlet excited states are n−π*, n−π*, π−π*, and π−π* in increasing order of energy. Higher excited states of *p*-BQ were studied experimentally by Brint et al.[7c] and theoretically by Pou-Amérigo et al.[11c] and Weber et al.[11d] Recent CASPT2 calculations[11c,d] provided the assignments of Rydberg excited states as well as valence excited states.

Assignments of the ionized states of *p*-BQ are not yet final, and the order of ionization energies has been controversial.[11b,12] Almost all theoretical studies on ionizations are due to Koopmans theorem and only very few calculations including electron correlations have been reported. Ha performed SDCI and MR−SDCI calculations with double-ζ basis set.[11b] He assigned the lowest four ionized states to n, n, π, and π and supported the assignments by Dougherty and McGlynn[12c] and Åsbrink et al.[12b] Recently, Stanton et al.[12d] reported a high-resolution photoelectron spectrum and analyzed it using EOMIP−CCSD[13a] and linear response CC3 calculations[13b] for the four lowest ionized states. They also proposed n, n, π, and π states as the lowest four ionized states. For higher ionized states, however, the calculated values were in poor agreement with the experimental values, and the assignments were different from those given in the literature.[10b,11b,12b,14] Although Ha calculated eight ionized states, explicit assignments to the experimental values were done only for the lowest four states.[11b] The assignment of higher ionized states of *p*-BQ is, therefore, still an open question.

For the anion radical of *p*-BQ, various experimental values of electron affinity have been reported,[15] with the recent one being 1.86 eV.[15d] The excited states of the anion radical have

* To whom correspondence should be addressed.

10.1021/jp013166a CCC: $22.00
Published on Web 03/19/2002

also been observed in various spectra.[16] The excited states corresponding to the vertical excitations at the geometry of the anion ground state were observed in aqueous solution by resonance Raman spectroscopy (RRS),[16a] in gas phase by electron photodetachment spectroscopy (EPDS),[15c,15d] and in 2-methyltetrahydrofuran (MTHF) by electronic absorption spectroscopy (EAS)[16b] and by fluorescence spectroscopy (FS).[16c] On the other hand, the spectroscopy that is due to the electron scattering technique gives the vertical excitation energies at the geometry of the neutral ground state. For the *p*-BQ anion radical, electron transmission spectroscopy (ETS),[16d,16e] electron energy loss spectroscopy (EELS),[16f] and SF_6 scavenger spectroscopy (SF_6SS),[15a] all in gas phase, have been reported. However, the assignment even for the lowest symmetry-allowed excited state is still controversial: it lies in the energy region 0.7−0.95 eV above the neutral ground state. There are two candidates for this state: one is ^2A_u state that is the excitation from the π^*_{SOMO} orbital of the anion radical to a higher unoccupied π^* orbital, and the other is $^2B_{3u}$ state that is the excitation from a doubly occupied π orbital to the π^*_{SOMO} orbital. Therefore, an aim of this paper is to give a definite assignment of the lowest allowed excited state.

Higher excited states at the anion geometry were observed by RRS,[16a] EPDS,[15c] and EAS,[16b] independently. The RRS and EAS studies found at least two states other than the first allowed state in the region of 3.4−4.0 eV above the anion ground state. At the neutral geometry, two states were reported above the first one by SF_6SS,[15a] ETS,[16d,16e] and EELS,[16f] and their excitation energies were at about 1.5 and 2.1 eV, respectively. The assignments of these states are not yet established as well as the first excited state.

At the anion geometry, symmetry-forbidden states below the lowest allowed state were reported by EPDS[15d] and by FS[16c] independently. Cook et al. found the emission band edge at 0.5 eV below the absorption band in their fluorescence spectra and concluded that there exists an optically forbidden transition below the lowest allowed state.[16c] Schiedt et al. observed several peaks of about 1ps lifetimes at 2.2−2.4 eV and also concluded the existence of two or one forbidden state(s) there.[15d] Both authors assigned such states to the transitions from doubly occupied n orbital to π^* SOMO, though they also noted their assignments not to be conclusive because of the difficulty in observing their vibronic features because of the absence of the origin transitions intrinsic to Herzberg−Teller coupling and the small energy difference of these electronic states.

On the theoretical side, several studies have been published on the excited states of the *p*-BQ anion radical. As ab initio calculations, MP2,[16c] CASSCF,[17a] and CASPT2[17b] studies have been reported. MP2 calculations by Cook et al.[16c] found two forbidden $n-\pi^*_{SOMO}$ transitions below the $\pi^*_{SOMO}-\pi^*$ (^2A_u) transition at the anion geometry. They assigned the experimentally observed forbidden states to two $n-\pi^*_{SOMO}$ states and the lowest allowed state to the $\pi^*_{SOMO}-\pi^*$ (^2A_u) transition, respectively, but they did not calculate higher excited states. Wheeler calculated the ground and five low-lying excited states of the anion radical by CASSCF method.[17a] (Although in his paper he did not explicitly state which geometry was employed, it is expected to be the anion ground-state geometry.) The CASSCF calculations provided the $\pi-\pi^*_{SOMO}$ ($^2B_{3u}$) state lower than the $\pi^*_{SOMO}-\pi^*$ (^2A_u) state, and it was concluded that the lowest allowed state was $^2B_{3u}$. Recent CASPT2 calculations[17b] at the anion geometry also supported this conclusion: the calculated energy difference between the $^2B_{3u}$ and ^2A_u states were, however, only a few hundredths of an eV, and furthermore, ^2A_u was more stable than $^2B_{3u}$ at the neutral geometry. Thus, both experimentally and theoretically, the assignments of the excited states of the *p*-BQ anion radical are indefinite.

For reliable theoretical assignments of the spectra, one should use highly accurate theory with a large basis set. The symmetry adapted cluster (SAC)[18]/SAC−configuration interaction (CI)[19] method is a powerful theory to describe ground and excited states and has been applied to various systems.[20] The SAC/SAC−CI method is applicable to the ground and excited states of various electronic species (neutral states, ionized states, and electron attached states) with a similar accuracy. This property is particularly important for the present study of *p*-BQ: we study here the ground and excited states of *p*-BQ, the ionization spectra of *p*-BQ below 20 eV, and the ground and electronic excited states of the *p*-BQ anion radical observed by several experiments. The calculated excitation and ionization energies showed good agreement with experiments, indicating that our assignments are reasonable. We would like to clarify the above-mentioned situations in the assignment of the electronic excited states.

2. Calculational Method

We calculate by the SAC/SAC−CI method the ground state, singlet excited states, and doublet ionized states of *p*-BQ ($C_6H_4O_2$) and the doublet ground and excited states of *p*-BQ anion radical. The basis set we used was Huzinaga−Dunning's (9s5p/4s)/[5s3p/3s] with standard scaling factors[21] plus Huzinaga's polarization functions[22] ([2d] for C and O, [1p] for H), Dunning's diffuse anion basis[23] ([1s1p] for C, [2s2p] for O), and Dunning's Rydberg functions[23] (3s, 3p, and 3d functions of carbon split to [2s2p2d] with standard splitting factors). The Rydberg functions were put at the center of the molecule. The total number of the contracted basis functions was 292. The molecular geometry of neutral *p*-BQ is due to the electron diffraction experiments,[24] whereas for the *p*-BQ anion radical the geometry was optimized by UMP2/[5s3p/3s]+pol.(d,p)+diff.(s,p) calculations.

We used the SAC/SAC−CI SD-*R* method in which one- and two-electron excitation operators are considered as linked operators. Hartree−Fock (HF) orbitals were used as reference orbitals. The active space consisted of 20 occupied orbitals and 256 unoccupied orbitals, and only 1s orbitals were frozen as core orbitals. All of the single excitation operators and part of the double excitation operators selected by the perturbative selection procedure[25] were employed as linked operators. The selection thresholds were 1×10^{-5} and 1×10^{-6} for the ground and excited states, respectively. For the unlinked operators, S_2^2, R_1S_2, and R_2S_2 types were employed, where S_n is a symmetry-adapted *n*-electron excitation operator for the SAC calculation and R_n is the same one for the SAC−CI calculation. Selection thresholds for the unlinked terms were $\tau_g = 0.002$ (0.005 for singlet states), $\tau = 0.001$, $\tau_s = \tau_d = 0.05$ (0.0, 0.005 for *p*-BQ anion radical, respectively); the details of these thresholds were described elsewhere.[25,26] All calculations were carried out by using the local version of the SAC−CI program[26] combined with the Gaussian 98 program package.[27]

3. Singlet Ground and Excited States of *p*-BQ

The energies and natures of some of the HF orbitals of neutral *p*-BQ are listed in Table 1. Figure 1 shows some important ones. We define the *z* axis on the line connecting two carbonyls and the *x* axis as the direction perpendicular to the molecular plane. (Confusingly, some papers are employing different definitions from ours. In our paper, however, all of the symmetry

TABLE 1: Orbital Energies and Natures of Some HF Orbitals of Neutral *p*-BQ

MO number[a]	symmetry[b]	orbital energy [eV]	nature[c]
		Occupied Orbitals	
14	$2b_{3g}$	−23.826	σ_g^-, n_g^-
15	$6a_g$	−22.733	σ_g^+
16	$3b_{2u}$	−19.559	n_u^+, σ_u^+
17	$7a_g$	−19.456	σ_g^+
18	$6b_{1u}$	−18.799	n_u^-, σ_u^-
19	$4b_{2u}$	−17.554	σ_u^+
20	$7b_{1u}$	−17.203	n_u^-
21	$8a_g$	−16.441	σ_g^+, n_g^+
22	$1b_{3u}$	−16.222	π_u^+
23	$3b_{3g}$	−15.994	n_g^-, σ_g^-
24	$1b_{2g}$	−15.071	π_g^-
25	$5b_{2u}$	−12.676	n_u^+
26	$4b_{3g}$	−12.171	n_g^-
27	$2b_{3u}$	−11.299	π_u^+
28	$1b_{1g}$	−11.199	π_g^+ (HOMO)
		Unoccupied Orbitals	
29	$2b_{2g}$	−0.010	π_g^-* (LUMO)
41	$1a_u$	2.546	π_u^-*
65	$7b_{3u}$	5.255	π_u^+*

[a] The numbering starts from the lowest energy orbital including the core orbitals. [b] See Figure 1 and the text for the definition of molecular axes. [c] The subscripts g and u stand for the symmetry for the inversion center, and the superscripts + and − stand for the symmetry with respect to the *xy* plane in Figure 1.

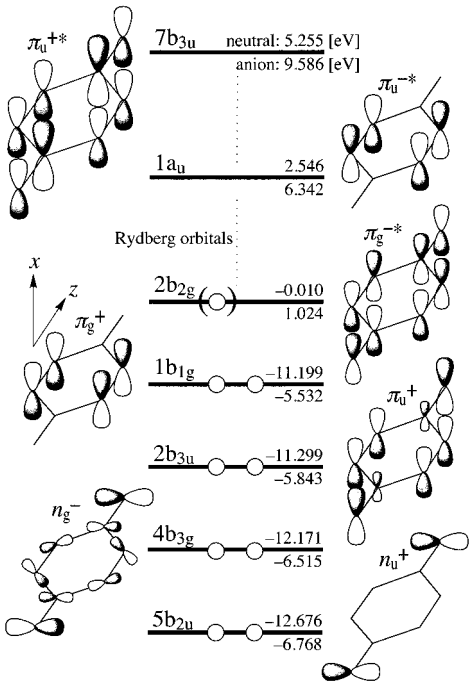

Figure 1. Some important Hartree−Fock molecular orbitals and their energies of *p*-BQ and its anion radical. The molecular axes are shown in the figure. Subscripts g and u stand for the symmetry for the inversion center, and superscripts + and − stand for the symmetry for the *xy* plane of the molecule. LUMO of neutral *p*-BQ ($2b_{2g}$; π_g^-*) is to be SOMO for the anion radical.

representations in the literature are hereafter translated to our definition.) The occupied orbitals from HOMO are π_g^+ (#28; $1b_{1g}$), π_u^+ (#27; $2b_{3u}$), n_g^- (#26; $4b_{3g}$), and n_u^+ (#25; $5b_{2u}$). (Subscripts g and u stand for symmetric and anti-symmetric characters for the inversion center, respectively, and superscripts +, − stand for the same but for the *xy* plane of the molecule.) LUMO of *p*-BQ is π_g^-* (#29; $2b_{2g}$), which is to be SOMO for the anion radical. Two π_u^-* (#41; $1a_u$) and π_u^+* (#54; $7b_{3u}$) orbitals exist in the unoccupied higher energy region, and there are many Rydberg orbitals among these orbitals. Figure 1 also shows the orbital energies for the anion radical calculated by the open-shell RHF method.

Table 2 shows the singlet excitation energies of *p*-BQ and their natures calculated by the SAC/SAC−CI method. Experimental[7a,c,d,8] and calculated values[11c,d] in the literature are also listed in Table 1. In accordance with the results reported in the literature,[7,8,10] the excitation energies of the lowest four states were calculated to be n_g^-−π_g^-*$_{LUMO}$, n_u^+−π_g^-*$_{LUMO}$, π_g^+−π_g^-*$_{LUMO}$, and π_u^+−π_g^-*$_{LUMO}$ in increasing energy order, though the HOMO is π_g^+ MO and n MOs are deeper in energy (Figure 1). The origin of this exchange is not due to electron correlations but to large orbital relaxations in the excited states because even SECI exhibits similar solutions. The energy differences between the two n−π* states and between the two π−π* states were 0.19 and 0.95 eV, respectively, and these differences were also reversed as compared with the corresponding HF orbital energy differences, 0.50 and 0.10 eV, respectively. The present calculated values are in rather good agreement with the experimental values and give the same assignments of the vertical excited states as the previous CASPT2 calculations.[11c,d]

4. Ionized States of *p*-BQ

For ionized states, we performed the perturbation selection of linked operators, using not only the single reference configurations but also the single and double reference configurations. We confirmed that both single- and SD-reference calculations gave similar results. Calculational results are shown in Table 3, in which the experimental[12a,b] values and other calculated values[11b,12d] found in the literature are also listed. We show in Figure 2 the theoretical ionization spectrum obtained by the SAC/SAC−CI calculations together with the experimental spectra reported by Brundle et al.[12a] and Åsbrink et al.[12b] The intensities of the peaks were calculated by the monopole approximation.[28] The calculated spectra show good agreement with the experimental ones, and therefore, we believe that the assignments of the ionization peaks up to 20 eV given in Table 3 should be reliable. All of the peaks up to 20 eV are mainly due to one-electron ionization processes, and therefore, the effect of the "shake-up" processes to the spectra would be small.

For *p*-BQ, the Koopmans theorem gives wrong ordering of the ionization peaks. The calculated order of the ionized states by the SAC−CI method were n_g^- ($^2B_{3g}$), n_u^+ ($^2B_{2u}$), π_u^+ ($^2B_{3u}$), and π_g^+ ($^2B_{1g}$) in increasing energy order (Table 3), whereas they were π_g^+, π_u^+, n_g^-, and n_u^+ by the Koopmans theorem (Figure 1). The SAC−CI result agrees with the assignments by Ha (MR−SDCI/DZ),[11b] by Åsbrink et al.[12b] (experimental and HAM/3 semiempirical MO method[29]) and by Stanton et al.[12d] (EOMIP−CCSD,[13a] LRCC3 method,[13b] and the simulations with linear vibronic coupling (LVC) model[30]), though the interpretations on the order of the two π states by HAM3 calculations and by the LVC model are different from ours. The energy reversal of the n and π states between the HF and SAC/SAC−CI methods is attributed to electron correlations as Ha pointed out. Thus, the origin of the reversal is different from the case of singlet excited states in which it is attributed to orbital relaxations.

The ionization peaks (and shoulders) in the energy region higher than 13 eV of the observed spectra are corresponded to the calculated states one-by-one and were assigned to n_g^-, π_g^-, n_g^+, n_u^-, π_u^+, σ_u^+, σ_u^-, σ_g^+, σ_u^+, σ_g^+, and σ_g^- states in

TABLE 2: Excitation Energies and Natures of Singlet Excited States of *p*-BQ

	SAC−CI				experimental		CASPT2	
states[a]	main configuration ($\|C\| > 0.3$)	nature[a]	excitation energy [eV]	oscillator strength	excitation energy [eV]	oscillator strength	excitation energy [eV]	oscillator strength[b]
1^1B_{1g}	0.89(26−29)	$n_g^- - \pi_g^*{}_{LUMO}$	2.51	0.0	2.49[c,d]		2.50[e], 2.39[f]	0.0
1^1A_u	0.90(25−29)	$n_u^+ - \pi_g^*{}_{LUMO}$	2.70	0.0	2.52[c], 2.48[d]		2.50[e], 2.43[f]	0.0
1^1B_{3g}	0.95(28−29)	$\pi_g^+ - \pi_g^*{}_{LUMO}$	4.52	0.0	4.07[c], 4.4[g], 4.6[h]	0.005 ± 0.001[h]	4.19[e], 4.01[f]	0.0
1^1B_{1u}	0.93(27−29)	$\pi_u^+ - \pi_g^*{}_{LUMO}$	5.47	0.704[i]	5.12[c], 5.1[g], 5.4[h]	0.44 ± 0.05[h]	5.15[e], 5.09[f]	0.616[e], 0.636[f]

[a] See the footnote of Table 1 for the notations. [b] Estimated using the transition moments calculated by CASSCF. [c] Reference 7a. (0−0 transition) [d] Reference 7d. (0−0 transition) [e] Reference 11c. [f] Reference 11d. [g] Reference 8. (Band maxima of the states were taken.) [h] Reference 7c. (Band maxima of the states were taken.) [i] The calculation without diffuse anion bases on carbon atoms.

TABLE 3: Energies and Natures of the Ionized States of Neutral *p*-BQ

	SAC−CI				excitation energy in other studies [eV]		
states[a]	main configurations ($\|C\| > 0.3$)	nature[a]	ionization energy [eV]	intensity[b]	exptl.	MR−SDCI/DZ[c]	EOMIP−CCSD LPCC3[d]
1^2B_{3g}	0.94(26)	n_g^-	9.57	0.898	10.11[e], 10.0[f]	9.06	10.05 ± 0.10
1^2B_{2u}	0.94(25)	n_u^+	9.91	0.893	10.41[e], 10.3[f]	9.26	10.30 ± 0.10
1^2B_{3u}	0.96(27)	π_u^+	10.66	0.931	11.06[e], 10.9[f]	10.35	11.15 ± 0.10
1^2B_{1g}	0.97(28)	π_g^+	10.91	0.944	11.5[e], 11.0[f]	10.5	11.05 ± 0.20
2^2B_{3g}	0.93(23)	n_g^-, σ_g^-	13.50	0.903	*13.4*[e,g], *13.3*[f,g]	12.72	
1^2B_{2g}	0.92(24) − 0.32(27−29,27)	π_g^-	13.59	0.844	13.43[e], 13.5[f]	12.95	
1^2A_g	0.94(21)	n_g^+, σ_g^+	14.02	0.913	14.3[e], *14.3*[f,g]	14.25	
1^2B_{1u}	0.89(20) − 0.33(18)	n_u^-, σ_u^-	14.63	0.901	14.7[e], *14.8*[f,g]		
2^2B_{3u}	0.93(22)	π_u^+	14.77	0.872	14.8[e], 14.9[f]	14.3	
2^2B_{2u}	0.94(19)	σ_u^+	15.55	0.907	15.3[e], 15.5[f]		
2^2B_{1u}	0.88(18) + 0.35(20)	σ_u^-, n_u^-	16.26	0.907	*16.2*[e,g],16.2[f]		
2^2A_g	0.92(17)	σ_g^+	16.73	0.887	16.6[e], 16.7[f]		
3^2B_{2u}	0.92(16)	σ_u^+, n_u^+	16.81	0.875	17.0[f]		
3^2A_g	0.90(15)	σ_g^+	19.82	0.816	19.5[f]		
3^2B_{3g}	0.68(27−29,25) + 0.34(27−65,26)	$n_u^+, \sigma_u^+ - \sigma_g^+$*	20.32	0.062			
4^2B_{3g}	0.79(14)	σ_g^-, n_g^-	20.83	0.621	20.1[f]		

[a] See the footnote of Table 1 for the notations. [b] Estimated using the monopole approximation. [c] Reference 11b. [d] Reference 12d. "Best theoretical estimate" values according to the authors of ref 12d. [e] Reference 12a. [f] Reference 12b. [g] The values in italic are those of shoulder peaks.

increasing order of energy. Our assignments are different from any of the reported calculations. Our calculations, however, agree with the experimental spectra much better than any of the reported ones, and we therefore believe that our assignments are correct. Although MR−SDCI/DZ calculations by Ha[11b] also provided the same order of the ionized states as ours, he did not give explicit assignments to the experimental values.

5. Ground and Excited States of the *p*-BQ Anion Radical

Theoretical studies on the excited states of the *p*-BQ anion radical have a difficulty in describing doublet-to-doublet transitions, because they include various types of electron promotions which often consist of two-electron processes from the closed-shell structures even if actual promotions are one-electron processes. To calculate such excited states using the SAC/SAC−CI method, we classified anionized states into three types. Type I includes the states whose main configurations are represented by electron promotions from SOMO to higher unoccupied orbitals. Such excitations can be described by one-electron attachment to the neutral *p*-BQ. Type II includes the states represented mainly by promotions from doubly occupied orbitals to SOMO. They can be described as one-electron ionizations from the *p*-BQ dianion. Type III includes the states represented mainly as electron promotions from doubly occupied orbitals to unoccupied ones. They cannot be described by one-electron processes from the closed-shell systems. These three types of excitations are illustrated in Figure 3.

Here it is worthwhile to refer to the relationship between these excitation types and the two resonance mechanisms, shape and Feshbach resonances. For the *p*-BQ anion radical, types I and II correspond to shape and Feshbach resonances, respectively. All of the valence excited states of the *p*-BQ anion lie above the electron detachment threshold, namely, above the energy of the neutral *p*-BQ. This means that these excited states of the anion are not bound states but metastable and are observed only as resonance states. The detachment from every type I excited state gives the neutral ground state, as seen from Figure 3, and therefore, type I excitations must induce shape resonances. On the other hand, the detachments from type II excited states produce neutral excited states, not the ground state, and therefore, the shape resonance would occur when the excited state of the anion has a higher energy than the neutral system, whereas the Feshbach resonance would occur in the contrary cases. For *p*-BQ, the lowest excited state is located at about 2.5 eV above the neutral ground state. As seen later, four low-lying type II excited states were calculated to lie below this excited state, and therefore, these type II excitations would be associated with Feshbach resonances.

Types I and II excited states are easily calculated by the SAC−CI SD-*R* method, and type III excited states are calculated accurately by the SAC−CI general-*R* method.[20b,31] Although we calculated the excited states of the *p*-BQ anion also by the general-*R* method with the double-ζ basis set, no new excited states appeared within 5 eV above the ground state of the *p*-BQ anion radical: we conclude that there are no type III valence excited states in this energy region. Therefore, we consider here in details only the types I and II excited states.

5.1. Ground State of the *p*-BQ Anion Radical. We employed open-shell restricted HF-MOs of the *p*-BQ anion radical as reference orbitals of both types of calculations, because here we are interested in the ground and excited states of the *p*-BQ anion radical and the reference orbitals should be

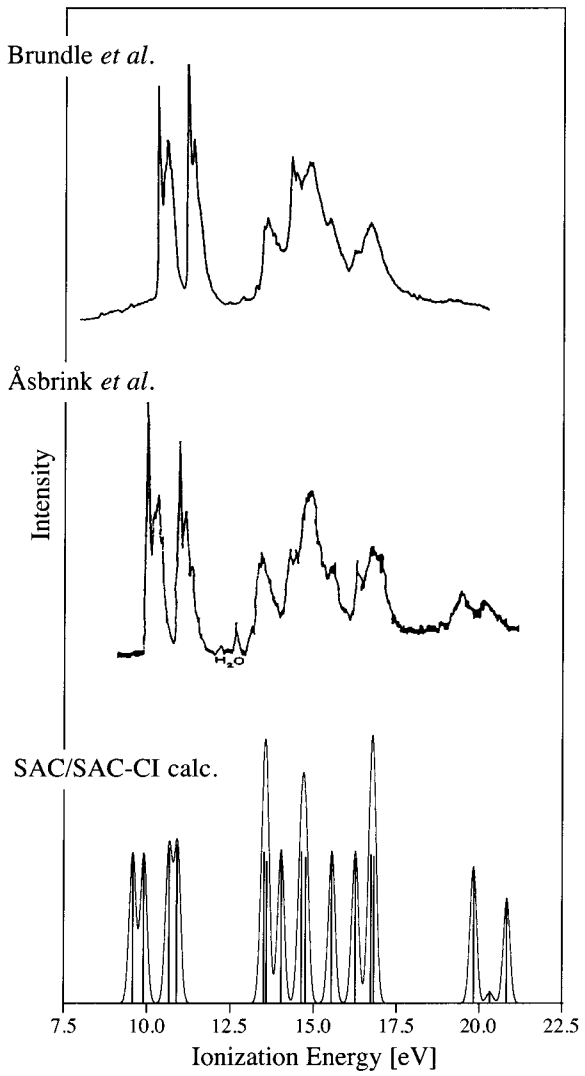

Figure 2. SAC−CI ionization spectrum compared with the experimental spectra observed by Brundle et al.[12a] and Åsbrink et al.[12b]

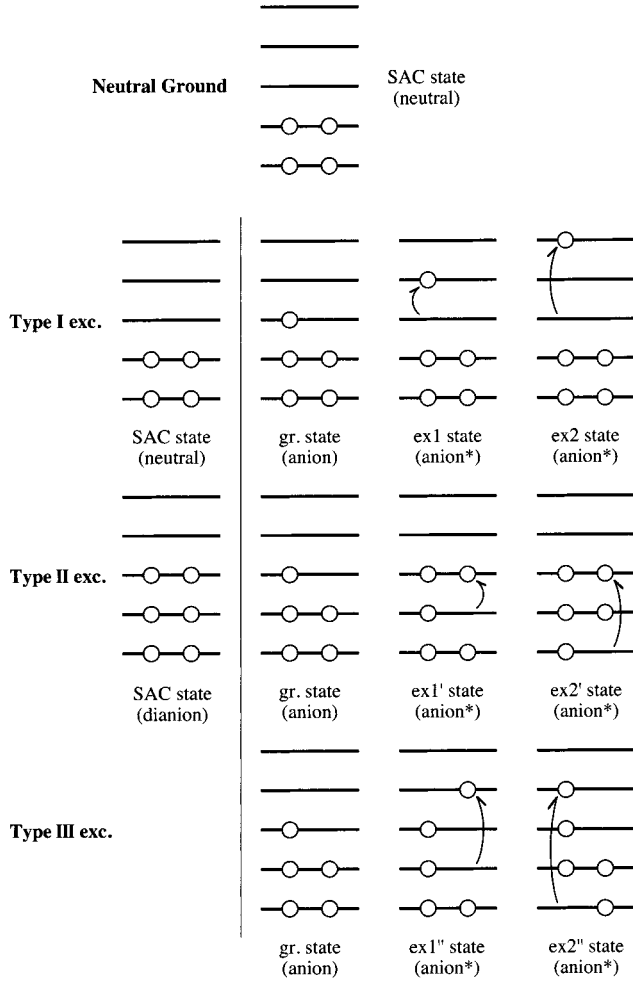

Figure 3. Three types of excitations in the anion radical of *p*-BQ. As for this system, types I and II excited states correspond to shape and Feshbach resonances, respectively.

optimized for the ground state of the anion. In these calculations, the ground state is represented as a SAC−CI state, not as a SAC state (see Figure 3). The SAC states for the *p*-BQ anion are used just as formal reference closed-shell states and therefore have little physical interest in both types of calculations. The electron affinity is described as the energy difference between the ground state of the anion radical obtained by the SAC−CI calculations and the "real" neutral ground state obtained by the SAC calculations referring to closed-shell HF MOs at the geometry of the neutral molecule. The SAC−CI calculations of the anion were performed using both neutral and anion geometries of the molecule. Note that the states described by types I and II excitations should be calculated in the same accuracy. The SAC/SAC−CI method satisfies such transferability.

The energies and natures of the some open-shell restricted HF orbitals of the *p*-BQ anion radical at the optimized geometry for the anion are listed in Table 4. The shapes and energies of the important orbitals are shown in Figure 1. The occupied orbitals from the highest doubly occupied MO are π_g^+ (#28; $1b_{1g}$), π_u^+ (#27; $2b_{3u}$), n_g^- (#26; $4b_{3g}$), and n_u^+ (#25; $5b_{2u}$), which are the same as in the case of neutral *p*-BQ, and one electron is accommodated in π_g^-* (#29; $2b_{2g}$), which is SOMO. The ground state of the *p*-BQ anion radical is therefore $^2B_{2g}$. The π_u^-* (#51; $1a_u$, #64; $2a_u$) and π_u^+* (#54; $5b_{3u}$, #69; $7b_{3u}$) orbitals exist in the unoccupied higher energy region, and there are many orbitals with diffuse characters among these orbitals. The situation is thus similar to that of neutral *p*-BQ. The ROHF orbitals of the anion at the neutral geometry are also quite similar to those at the anion geometry.

The optimized geometry for the anion radical had longer C═O and C═C bonds and shorter C−C bonds than the neutral (experimental) geometry. The C═O, C═C, and C−C bonds at the neutral geometry were reported to be 1.225, 1.344, and 1.481 Å, respectively,[24] whereas for the anion, they were calculated to be 1.268, 1.371, and 1.448 Å, respectively. These geometry variations can be simply explained in terms of the shape of the SOMO of the anion, as pointed out in many papers. The SOMO has antibonding natures on the C═C and C═O bonds and bonding natures on the C−C bonds. An electron accommodation to the SOMO causes a decrease in the C═C and C═O bond orders and an increase in the C−C bond orders and, therefore, provides such geometry variations.

The adiabatic electron affinity was calculated to be 1.96 eV, which is comparable to the experimental values, 1.86,[15d] and 1.89,[15a] and 1.99 eV.[15b] On the other hand, our calculations provided 1.57 eV for the vertical electron affinity at the neutral geometry, and therefore, the effect of the geometry rearrangement was estimated to be 0.39 eV.

5.2. Excited States of the *p*-BQ Anion at the Anion Geometry. The excitation energies and their natures calculated by the SAC−CI method at the optimized anion geometry are

TABLE 4: Orbital Energies and Natures of Some ROHF Orbitals of the *p*-BQ Anion Radical

MO number[a]	symmetry[a]	orbital energy [eV]	nature[a]
	Occupied Orbitals		
25	$5b_{2u}$	−6.768	n_u^+
26	$4b_{3g}$	−6.515	n_g^-
27	$2b_{3u}$	−5.843	π_u^+
28	$1b_{1g}$	−5.532	π_g^+
29	$2b_{2g}$	1.024	π_g^-* (SOMO)
	Unoccupied Orbitals		
30	$9a_g$	2.152	diff(s)[b]
31	$10a_g$	2.774	diff(s)
32	$5b_{3g}$	2.829	diff(d_{yz}), σ_g^-*
33	$2b_{1g}$	2.890	diff(d_{xy})
34	$3b_{2g}$	2.927	diff(d_{xz})
35	$11a_g$	2.950	diff(s), σ_g^+*
36	$6b_{2u}$	3.118	diff(p_y)
37	$8b_{1u}$	3.200	diff(p_z), σ_u^-*
38	$3b_{3u}$	3.301	diff(p_x)
39	$12a_g$	3.725	diff(s), σ_g^+*
40	$13a_g$	5.251	diff(s), σ_g^+*
41	$6b_{3g}$	5.431	diff(d_{yz})
42	$9b_{1u}$	5.580	diff(p_z), σ_u^-*
43	$4b_{2g}$	5.612	diff(d_{xz})
44	$14a_g$	5.645	diff(s), σ_g^+*
45	$3b_{1g}$	5.718	diff(d_{xy})
46	$10b_{1u}$	5.765	diff(p_z), σ_u^-*
47	$7b_{2u}$	5.978	diff(p_y), σ_u^+*
48	$8b_{2u}$	6.165	diff(p_y), σ_u^+*
49	$4b_{3u}$	6.284	diff(p_x)
51	$1a_u$	6.342	π_u^-*
54	$5b_{3u}$	6.662	diff(p_x), π_u^+*
64	$2a_u$	8.319	π_u^-*
69	$7b_{3u}$	9.586	π_u^+*

[a] See the footnote of Table 1 for the notations. [b] "diff" stand for the character in which diffuse anion functions are predominant.

shown in Table 5, in which the experimental[15c,d,16b,c] excitation energies (and adiabatic electron affinities) in the literature are also listed. The experimental values in Table 5 are placed according to our assignments. All of the excitation energies in Table 5 are those from the anion ground state ($^2B_{2g}$). There are six valence excited states in this energy region. 1^2B_{3g}, 2^2B_{2u}, 2^2B_{3u}, and 2^2B_{1g} states are formed by the type II (doubly occupied orbitals → SOMO) excitations: they are Feshbach resonance states. Other states are due to the type I (SOMO → higher unoccupied orbitals) excitations: they are shape resonance states.

Lowest Symmetry-Allowed State. Table 6 shows the excitation energies of the *p*-BQ anion radical at the anion geometry obtained by various experimental and theoretical methods. The assignments in Table 6 are due to the original authors. The abbreviations of the experimental methods are explained in the footnotes of Table 5.

The lowest symmetry-allowed state has been observed experimentally at 2.5−3.0 eV above the anion ground state. It has been assigned to either ^2A_u ($\pi^*_{SOMO}-\pi^*$ shape resonance) or $^2B_{3u}$ ($\pi-\pi^*_{SOMO}$ Feshbach resonance). The EPDS and FS experiments and the SAC−CI and MP2 calculations support ^2A_u, whereas the RRS experiments and the CASSCF and CASPT2 calculations support $^2B_{3u}$.

The assignment to ^2A_u by Schiedt et al. from EPDS[15d] were mainly based on the lifetime of the first peak having a large intensity. The first intense state at 2.5 eV above the anion ground-state had a very short lifetime, which was about 25 fs and was less than a tenth of those of other peaks at 2.2−2.4 eV. This implies that the state at 2.5 eV would be a shape resonance state because the Feshbach resonance is a two-electron process and should require longer time for the electron detachment process. Furthermore, their analyses on the vibronic states by photodetachment photoelectron spectroscopy (PD-PES) and the unpublished CASPT2 result also supported the assignment that this state is ^2A_u shape resonance state.[15d] Thus, this assignment seems to be reasonable.

On the other hand, Tripathi et al. observed four peaks at 2.90, 3.06, 3.35, and 3.94 eV above the anion ground state by EAS in aqueous solution and assigned them to $^2B_{3u}$, ^2A_u, and $^2B_{3u}$ electronic excited states in the energy increasing order, with the support of the resonance Raman spectroscopy (RRS).[16a] (The peak at 3.06 eV was assigned to the vibrational feature of the $^2B_{3u}$ state at 2.90 eV.) They found large resonances in the vibrational modes of the C=C stretch, C=O stretch, and C−H bending at 2.88 eV, whereas the intensity of the ring breathing mode became larger as the energy increased and reached its maximum at 3.35 eV. When the Franck−Condon factors between each excited state and the ground state of the anion are considered, it is expected that the $^2B_{3u}$ Feshbach resonance state would favor the C=C and C=O stretch because both the electron removal from $2b_{3u}$ MO and the electron accommodation into $2b_{2g}$ SOMO result in an elongation of the C=C and C=O bonds. (See the shapes of these MO shown in Figure 1.) In contrast, the ^2A_u shape resonance state would favor the ring breathing mode because the excitation from SOMO to a_u MOs results in an elongation of the C=C and C−C bonds (and shrink of the C=O bonds). The CASSCF geometry optimizations for these two states performed by Pou-Amérigo et al.[17b] supported the above expectations: the optimized geometry for the $^2B_{3u}$ state has long C=C and C=O bonds, and that of the ^2A_u state has long C=C and C−C bonds compared with the anion ground-state geometry. This implies that the lowest allowed state is $^2B_{3u}$ and the second is ^2A_u. Furthermore, the recent CASSCF vibrational analysis by Pou-Amérigo et al.[17b] for these states supported the assignments by Tripathi et al. Their calculations demonstrated that the intense vibrational peaks of the $^2B_{3u}$ state are mainly due to the C=C and C−C stretch, whereas that of the ^2A_u state is due to the ring breathing and the C−H bending. They also showed that the $^2B_{3u}$ state has two strong vibrational bands including the 0−0 band like the peaks at 2.90 and 3.06 eV in the EAS, whereas the ^2A_u state does not have such vibrational structures. This also supports the assignments by Tripathi et al. to $^2B_{3u}$.

Then, which state is the lowest actually? We interpreted this problem as follows; in the gas phase, the ^2A_u state would be lower than the $^2B_{3u}$ state. However, in aqueous solution, the solvent effects of water would affect the energies of these states and as a consequence change the order of these states. Therefore, both of the experimental assignments would be correct for the peaks in their own spectra.

To investigate the validity of this assumption, we performed the SAC−CI calculations for the excited states of the *p*-benzosemiquinone (*p*-BQH) radical, which is formed by a proton attachment to the *p*-BQ anion radical. The solvent effect on the *p*-BQ anion in aqueous solution would be due to the formation of the hydrogen bond between one of the oxygen atoms of the *p*-BQ anion and a hydrogen atom of water: electrostatic multipole interactions of the anion with water would be weaker because *p*-BQ does not have a permanent dipole moment. *p*-BQH was regarded as an extreme sample of the hydrogen-bonded molecule. We employed the geometry such that the skeleton of the *p*-BQ anion radical was retained. The additional hydrogen was placed within the BQ molecular plane with R(O−H) = 1.0 Å and ∠(C−O−H) = 109.81°. We did not

TABLE 5: Ground and Excited States of the *p*-BQ Anion Radical at the Anion Geometry[a]

	SAC−CI					experimental values[b]			
states[c]	main configurations ($\|C\| > 0.3$)	nature[c]	exc. type	excitation energy [eV]	oscillator strength	EPDS[d] gas phase	EPDS[e] gas phase	EAS[f] in MTHF	FS[g] in MTHF
1^2B_{2g}		(anion ground state)		EA = 1.96[h]		1.99	1.86		
1^2A_g	0.86(29−30) − 0.43(29−39)	π_g^-*$_{SOMO}$−diff(s)	I	1.86	0.0				
1^2B_{2u}	0.95(29−36)	π_g^-*$_{SOMO}$−diff(p_y)	I	2.28	0.0				
1^2B_{3g}	0.94(26−29)	n_g^-−π_g^-*$_{SOMO}$	II	2.38	0.0		2.27		
1^2B_{3u}	0.94(29−38)	π_g^-*$_{SOMO}$−diff(p_x)	I	2.39	0.001				
2^2A_g	0.94(29−31)	π_g^-*$_{SOMO}$−diff(s)	I	2.43	0.0				
2^2B_{2u}	0.94(25−29)	n_u^+−π_g^-*$_{SOMO}$	II	2.44	0.0		2.41		
1^2B_{1u}	0.94(29−37)	π_g^-*$_{SOMO}$−diff(p_z), σ_u^-*	I	2.48	<0.001				
1^2B_{1g}	0.96(29−33)	π_g^-*$_{SOMO}$−diff(d_{xy})	I	2.50	0.0				
2^2B_{3g}	0.96(29−32)	π_g^-*$_{SOMO}$−diff(d_{yz}), σ_g^-*	I	2.51	0.0				
2^2B_{2g}	0.96(29−34)	π_g^-*$_{SOMO}$−diff(d_{xz})	I	2.57	0.0				
3^2A_g	0.91(29−35)	π_g^-*$_{SOMO}$−diff(s), σ_g^+*	I	2.59	0.0				
1^2A_u	0.75(29−51) − 0.62(29−64)	π_g^-*$_{SOMO}$−π_u^-*	I	2.71	0.063	2.95	2.50	2.71	2.72
4^2A_g	0.74(29−39) + 0.42(29−30) + 0.31(29−35)	π_g^-*$_{SOMO}$−diff(s), σ_g^+*	I	2.77	0.0				
2^2B_{3u}	0.93(27−29)	π_u^+−π_g^-*$_{SOMO}$	II	3.50	0.324			3.81	
3^2B_{3u}	0.64(29−69) − 0.61(29−49)	π_g^-*$_{SOMO}$−π_u^+*, diff(p_x)	I	3.74	0.076	3.98		4.02	
2^2B_{1g}	0.95(28−29)	π_g^+−π_g^-*$_{SOMO}$	II	3.75	0.0				
5^2A_g	0.83(29−40) − 0.31(29−44)	π_g^-*$_{SOMO}$−diff(s), σ_g^+*	I	3.84	0.0				
3^2B_{3g}	0.94(29−41)	π_g^-*$_{SOMO}$−diff(d_{yz})	I	4.23	0.0				
6^2A_g	0.79(29−44) + 0.35(29−40) − 0.32(29−39)	π_g^-*$_{SOMO}$−diff(s), σ_g^+*	I	4.24	0.0				
2^2B_{1u}	0.72(29−46) − 0.57(29−42)	π_g^-*$_{SOMO}$−diff(p_z), σ_u^-*	I	4.34	0.001				
3^2B_{2g}	0.93(29−43)	π_g^-*$_{SOMO}$−diff(d_{xz})	I	4.34	0.0				
3^2B_{2u}	0.77(29−47) − 0.53(29−48)	π_g^-*$_{SOMO}$−diff(p_y), σ_u^+*	I	4.40	0.0				
3^2B_{1g}	0.94(29−45)	$\pi_g^-$$_{SOMO}$−diff($d_{xy}$)	I	4.44	0.0				
4^2B_{3u}	0.62(29−49) − 0.57(29−54) + 0.35(29−69)	$\pi_g^-$$_{SOMO}$−diff($p_x$), π_u^+*	I	4.67	0.025				

[a] All excitation energies are those from the anion ground state. [b] EPDS = electron photodetachment spectroscopy, EAS = electronic absorption spectroscopy, FS = fluorescence spectroscopy, MTHF = 2-methyltetrahydrofuran. [c] See the footnotes of Tables 1 and 4 for the notations. [d] Reference 15c. [e] Reference 15d. [f] Reference 16b. [g] Reference 16c. [h] All electron affinities are adiabatic ones.

TABLE 6: Comparison of Excitation Energies and Assignments by SAC−CI with Those by Experimental and Other Theoretical Results: Ground and Valence Excited States of the *p*-BQ Anion Radical at the Anion Geometry[a]

experimental[b]					theoretical			
EPDS[c] gas phase	EPDS[d] gas phase	EAS[e] aq. solution	EAS[f] in MTHF	FS[g] in MTHF	SAC−CI[h]	CASSCF[i]	MP2[g]	CASPT2[j]
					Ground State ($^2B_{2g}$)[k]			
EA = 1.99	EA = 1.86				EA = 1.96			EA = 2.01
					Excited States			
	2.27 ($^2B_{2u}$ [F])				2.38 ($^2B_{3g}$ [F])	2.46 ($^2B_{2u}$ [F])	2.05 ($^2B_{3g}$ [F])	2.23 ($^2B_{2u}$ [F])
	2.41 ($^2B_{3g}$ [F])				2.44 ($^2B_{2u}$ [F])	2.74 ($^2B_{3g}$ [F])	2.16 ($^2B_{2u}$ [F])	2.25 ($^2B_{3g}$ [F])
2.95	2.50 (^2A_u [S])	2.90 ($^2B_{3u}$)	2.71	2.72 (^2A_u [S])	2.71 (^2A_u [S])	3.17 ($^2B_{3u}$ [F])	3.24 (^2A_u [S])	2.80 ($^2B_{3u}$ [F])
		3.35 (^2A_u)	3.81		3.50 ($^2B_{3u}$ [F])	3.23 (^2A_u [S])		2.82 (^2A_u [S])
3.98		3.94 ($^2B_{3u}$)	4.02		3.74 ($^2B_{3u}$ [S])	4.70 ($^2B_{3u}$ [S])		3.56 ($^2B_{3u}$ [S])
					3.75 ($^2B_{1g}$ [F])			3.25 ($^2B_{1g}$ [F])

[a] [S] and [F] stand for shape and Feshbach resonances, respectively. All excitation energies are those from the anion ground state. [b] See the footnotes of Table 5 for the abbreviations. [c] Reference 15c. [d] Reference 15d. The assignments were based on the lifetime of the state, CASPT2 calculations, and photodetachment photoelectron spectroscopy (PD-PES) of the vibronic states. [e] Reference 16a. The assignments were based on resonance Raman spectroscopy of the vibronic states. [f] Reference 16b. [g] Reference 16c. The assignments were based on MP2 calculations. [h] Present work. [i] Reference 17a. [j] Reference 17b. [k] All electron affinities are adiabatic ones.

optimize the geometry for *p*-BQH in order to eliminate the effect of the geometry variation. The basis set and calculational conditions were the same as those for the *p*-BQ anion radical except that the Rydberg functions were not added in this calculation.

Table 7 shows the energies and natures of the excited states of the *p*-BQH radical at the geometry of the ground state of the *p*-BQ anion radical. The shapes of π MOs of *p*-BQH were mostly retained, compared with those of the *p*-BQ anion. Although the molecular symmetry of D_{2h} was lowered to C_s, the $\pi-\pi^*$ states still had quasi-D_{2h} symmetry. The excitation energy of the $3^2A''$ ($\sim^2B_{3u}$) state was calculated to be 3.45 eV, and that of the $4^2A''$ ($\sim^2A_u$) state was 3.54 eV: the $^2B_{3u}$ state does not change its energy position compared to *p*-BQ, whereas the ^2A_u state becomes largely unstable, and consequently, the relative position of the two states has exchanged. Generally speaking, type I excited states tend to be unstabilized, whereas type II ones tend to be stabilized. In particular, the energy increase and decrease in the $4^2A''$ ($\sim^2A_u$) and $2^2A''$ ($\sim^2B_{1g}$) states, respectively, are remarkable. The $4^2A''$ ($\sim^2A_u$) state has $^2B_{1g}$-like configurations to some extent, and at the same time, ^2A_u-like configurations are also mixed by the $2^2A''$ ($\sim^2B_{1g}$) state owing to the addition of a proton and, by the symmetry lowering, though the extent of mixing is not so large. These configuration mixings make the $2^2A''$ ($\sim^2B_{1g}$) state stable relative to the $4^2A''$ ($\sim^2A_u$) state. This result for *p*-BQH supports our assumption that, through hydrogen bond, the water solvent may affect the relative positions of the ^2A_u shape resonance state and the $^2B_{3u}$ Feshbach resonance state of the *p*-BQ anion radical.

TABLE 7: Ground and Excited States of the *p*-BQH Radical at the *p*-BQ$^-$ Geometry[a]

	SAC−CI				
states[b]	main configurations[b] (|C| > 0.3)	nature[b]	exc. type	excitation energy [eV]	oscillator strength
$1^2A'$ ($\sim^2B_{3g}$)	0.94(26−29)	$n_{(C=)O}-\pi_g^{-}*_{SOMO}$	II	1.17	0.000
$2^2A''$ ($\sim^2B_{1g}$)	0.94(28−29)	$\pi_g^{+}-\pi_g^{-}*_{SOMO}$	II	3.00	0.003
$3^2A''$ ($\sim^2B_{3u}$)	0.92(27−29)	$\pi_u^{+}-\pi_g^{-}*_{SOMO}$	II	3.45	0.189
$4^2A''$ ($\sim^2A_u$)	0.75(29−36) − 0.37(29−48) − 0.35(29−35)	$\pi_g^{-}*_{SOMO}-\pi_u^{-}*$	I	3.54	0.049
$5^2A''$ ($\sim^2B_{3u}$)	0.53(29−51) − 0.49(29−42) + 0.32(29−35) + 0.31(29−45) − 0.39(27−29)	$\pi_g^{-}*_{SOMO}-\pi_u^{+}*$	I	3.95	0.063
$2^2A'$ ($\sim^2B_{2u}+{}^2B_{3g}$)	0.92(25−29)	$n_{(C-)OH,(C=)O}$, $\sigma-\pi_g^{-}*_{SOMO}$	II	5.01	0.000

[a] All excitation energies are those from the anion ground state, $1\ ^2A''$ ($\sim^2B_{2g}$). [b] See the footnotes of Tables 1 and 4 for the notations.

Two $n-\pi^*_{SOMO}$ states ($1^2A'$ and $2^2A'$) in Table 7 are also greatly affected by proton attachment. These energy variations are due to the symmetry lowering and to the energy variation of the n MO itself. The 25th MO ($5b_{2u}$ for the *p*-BQ anion) mixes with σ characters and becomes more stable. On the other hand, the 26th MO ($4b_{3g}$ for the *p*-BQ anion) localizes the electron cloud to have n character and becomes less stable. The large energy variations in the two $n-\pi^*_{SOMO}$ states are thus very natural.

Other Valence Excited States. Excited states with energies higher than the lowest allowed state (1^2A_u according to our assignment) at the anion geometry were observed experimentally by EAS of Shida et al. in MTHF,[16b] EAS of Tripathi et al. in aqueous solution,[16a] and EPDS of Commita et al.[15c] The observed excitation energies are summarized in Table 6. The peak and shoulder at 3.81 and 4.02 eV, respectively, in Shida's EAS[16b] are both assigned to $^2B_{3u}$. According to the intensities of the peaks, the lower one is the type II $\pi_u^{+}-\pi_g^{-}*_{SOMO}$ transition and the higher one is the type I $\pi_g^{-}*_{SOMO}-\pi_u^{+}*$ transition. The former corresponds to the Feshbach resonance because the energy is lower than that of the electron-detached $\pi-\pi^*_{LUMO}$ state ($^1B_{1u}$), and the latter corresponds to the shape resonance. Because the polarity of MTHF is smaller than that of water and ethanol, the state order is expected to be different from that in aqueous solution discussed in the previous subsection. Although our results seem to be lower than the observed excitation energies, this underestimation may be attributed to the solvent effect: this is also supported by the fact that the 1^2A_u state in MTHF matrix is higher than that in gas phase by Schiedt et al. (see Tables 5 and 6). Shida et al. observed several smaller peaks near the peaks at 2.71 and 3.81 eV. We assigned them to the vibronic features of each electronic state because no states with large oscillator strengths were calculated in this energy region. The state at 3.98 eV observed in EPDS by Commita et al.[15c] is assigned to the $^2B_{3u}$ shape resonance state ($\pi_g^{-}*_{SOMO}-\pi_u^{+}*$) owing to the excitation energy. For the EAS results by Tripathi et al.,[16a] we do not give explicit assignments because the state order might have been changed in aqueous solution as discussed above.

For the state below the first allowed state, the existence of the symmetry-forbidden states has been pointed out experimentally. Schiedt et al. observed several Feshbach states below the first allowed state in their EPDS.[15d] The FS of the *p*-BQ anion observed by Cook et al.[16c] also suggested the existence of the forbidden states 0.5 eV below the absorption band edge of the first allowed state. In accordance with these experiments, our calculations yielded two forbidden $n-\pi^*_{SOMO}$ states below the 1^2A_u state. The lower is the $n_g^{-}-\pi_g^{-}*_{SOMO}$ (1^2B_{3g}) state and the higher is the $n_u^{+}-\pi_g^{-}*_{SOMO}$ (2^2B_{2u}) states. Both are mainly formed by the type II excitations, and their energies are lower than those of the corresponding electron-detached $n-\pi^*_{LUMO}$ states ($^1B_{1g}$ and ^1A_u). They are therefore the Feshbach resonance states. In the spectra of Schiedt et al., there were at least six sharp peaks below the lowest allowed state, and they were at 2.21, 2.23, 2.27, 2.40, 2.41, and 2.43 eV above the ground state. They assigned the peaks to two or one $n-\pi^*_{SOMO}$ Feshbach state(s) and their accompanied vibronic features. CASSCF by Wheeler et al.,[17a] ZINDO/S and MP2 by Cook et al.,[16c] and CASPT2 by Pou-Amérigo et al.[17b] gave two $n-\pi^*_{SOMO}$ states at 2.0−2.8 eV. Also in our studies, two $n-\pi^*_{SOMO}$ states were calculated at 2.38 and 2.44 eV, and therefore, it is natural to assign them to $n-\pi^*_{SOMO}$ transitions. Our SAC−CI and MP2 calculations by Cook et al. provided the order of the two $n-\pi^*_{SOMO}$ states different from that by CASSCF by Wheeler et al. and CASPT2 calculations by Pou-Amérigo et al. In our results $^2B_{3g}$ state is lower than 2^2B_{2u} state, whereas the order is reversed in the CASSCF and CASPT2 results. It is difficult to determine which is correct, because the transitions to these states are induced by Herzberg−Teller coupling and their origin transitions cannot be observed in principle. Moreover, because their energies are so close, it is difficult to fit the experimental vibronic peaks in the Herzberg−Teller coupling scheme, and therefore, theoretically more accurate calculations are required.

5.3. Excited States of the *p*-BQ Anion Radical at Neutral Geometry. In the experiments in which temporary anion states are formed by electron impact, the peak positions correspond to the vertical excitations between the neutral ground and the anion excited states at the equilibrium geometry of the neutral ground state of the molecule. To assign the excited states of the anion observed by such experiments, we have to investigate the excited states vertical to the ground state of the neutral molecule.

Table 8 shows the ground and excited states of the *p*-BQ anion radical at the neutral geometry. The energy of every type II excited state is lower than that of the corresponding singlet or triplet excited state. All type II states are therefore Feshbach resonance states similarly to the case of the anion geometry. The excitation energies observed by several electron-scattering experiments are also listed in the table.

Geometrical Effects on the Excitation Energies. We first study the effect of the geometry variation on the energy of each state. We see that the energy ordering of some valence excited states at the neutral geometry is different from that at the anion geometry. Two type II $n-\pi^*_{SOMO}$ states (2^2B_{3g} and 2^2B_{2u}) becomes unstable compared with the first allowed state (1^2A_u). Two type II $\pi-\pi^*_{SOMO}$ states (3^2B_{3u} and 3^2B_{1g}) also become unstable, and consequently, the order of the two $^2B_{3u}$ states is reversed. The variations in the energy levels of the states are depicted in Figure 4.

This is due to the different magnitude of the geometrical effect in each state. Figure 4 shows that the energy variations of the type I excited states are small, whereas all type II excited states become unstable in the neutral geometry, and the energy variations are very large. The type I excitation includes an

TABLE 8: Ground and Excited States of the *p*-BQ Anion Radical at the Neutral Geometry[a]

	SAC−CI					experimental values[b]			
states[c]	main configurations ($\|C\| > 0.3$)	nature[c]	exc. type	excitation energy [eV]	oscillator strength	ETS[d] gas phase	ETS[e] gas phase	EELS[f] gas phase	SF_6SS[g] gas phase
1^2B_{2g}		(anion ground state)		EA = 1.57[h]					1.89[i]
1^2A_g	0.86(29−30) − 0.42(29−39)	π_g^-*$_{SOMO}$−diff(s)	I	−0.21	0.0				
1^2B_{2u}	0.95(29−36)	π_g^-*$_{SOMO}$−diff(p_y)	I	0.21	0.0				
1^2B_{3u}	0.95(29−38)	π_g^-*$_{SOMO}$−diff(p_x)	I	0.34	<0.001				
2^2A_g	0.94(29−31)	π_g^-*$_{SOMO}$−diff(s)	I	0.35	0.0				
1^2B_{1u}	0.95(29−37)	π_g^-*$_{SOMO}$−diff(p_z), σ_u^-*	I	0.41	<0.001				
1^2B_{1g}	0.97(29−33)	π_g^-*$_{SOMO}$−diff(d_{xy})	I	0.43	0.0				
1^2B_{3g}	0.96(29−32)	π_g^-*$_{SOMO}$−diff(d_{yz}), σ_g^-*	I	0.43	0.0				
2^2B_{2g}	0.95(29−34)	π_g^-*$_{SOMO}$−diff(d_{xz})	I	0.50	0.0				
3^2A_g	0.92(29−35)	π_g^-*$_{SOMO}$−diff(s), σ_g^+*	I	0.52	0.0				
4^2A_g	0.76(29−39) + 0.42(29−30)	π_g^-*$_{SOMO}$−diff(s), σ_g^+*	I	0.71	0.0				
1^2A_u	0.74(29−51) − 0.62(29−64)	π_g^-*$_{SOMO}$−π_u^-*	I	0.83	0.063	0.72	0.69	0.77	0.70
2^2B_{3g}	0.94(26−29)	n_g^-−π_g^-*$_{SOMO}$	II	1.09	0.0				
2^2B_{2u}	0.94(25−29)	n_u^+−π_g^-*$_{SOMO}$	II	1.22	0.0				
5^2A_g	0.85(29−40)	π_g^-*$_{SOMO}$−diff(s), σ_g^+*	I	1.76	0.0				
2^2B_{3u}	0.61(29−69) − 0.60(29−49) − 0.31(29−54)	π_g^-*$_{SOMO}$−π_u^+*, diff(p_x)	I	1.79	0.069	1.43	1.41	1.6	1.35
3^2B_{3g}	0.94(29−41)	π_g^-*$_{SOMO}$−diff(d_{yz})	I	2.16	0.0				
6^2A_g	0.81(29−44) − 0.32(29−39) + 0.30(29−40)	π_g^-*$_{SOMO}$−diff(s), σ_g^+*	I	2.18	0.0				
3^2B_{2g}	0.93(29−43)	π_g^-*$_{SOMO}$−diff(d_{xz})	I	2.27	0.0				
2^2B_{1u}	0.75(29−45) + 0.55(29−42)	π_g^-*$_{SOMO}$−diff(p_z), σ_u^-*	I	2.27	0.001				
3^2B_{2u}	0.83(29−47) − 0.44(29−48)	π_g^-*$_{SOMO}$−diff(p_y), σ_u^+*	I	2.33	0.0				
2^2B_{1g}	0.95(29−46)	π_g^-*$_{SOMO}$−diff(d_{xy})	I	2.43	0.0				
3^2B_{3u}	0.93(27−29)	π_u^+−π_g^-*$_{SOMO}$	II	2.44	0.288	2.15	2.11	2.0	1.90
4^2B_{3u}	0.66(29−49) − 0.55(29−54) + 0.33(29−69)	π_g^-*$_{SOMO}$−diff(p_x), π_u^+*	I	2.58	0.026				
3^2B_{1g}	0.94(28−29)	π_g^+−π_g^-*$_{SOMO}$	II	2.66	0.0				

[a] All excitation energies are those from the neutral ground state. [b] ETS = electron transmission spectroscopy, EELS = electron energy loss spectroscopy, SF_6SS = SF_6 scavenger spectroscopy. [c] See the footnotes of Tables 1 and 4 for the notations. [d] Reference 16d. [e] Reference 16e. [f] Reference 16f. [g] Reference 15a. [h] Vertical electron affinity. [i] Adiabatic electron affinity.

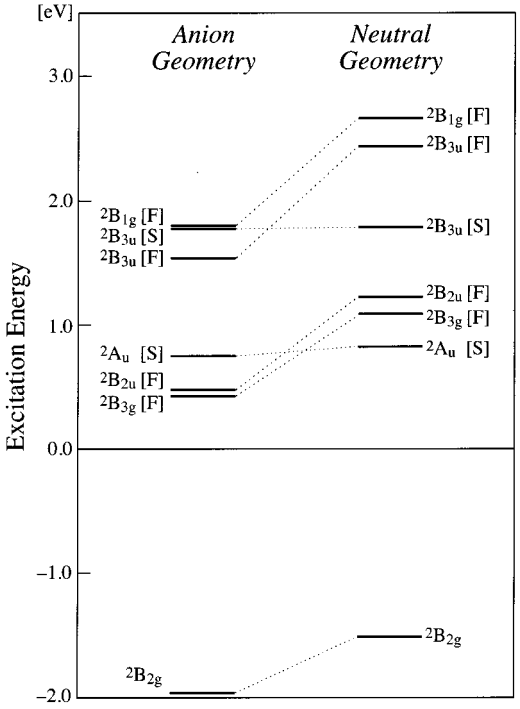

Figure 4. Geometrical effects on the energies of each state of the *p*-BQ anion radical. The energy origin is the singlet ground-state energy at the neutral geometry. [S] and [F] represent shape and Feshbach resonance states, respectively.

electron removal from the SOMO, whereas in the type II excitation, an electron is accommodated in the SOMO to make it a doubly occupied orbital. The geometry variation from the neutral to the anion one is mainly caused by the electron attachment to LUMO. Type I excited states therefore favor the nuclear relaxation from the anion to the neutral geometry. In contrast, the type II excited states favor the nuclear relaxation toward the anion geometry. Consequently, type II excited states are less stable at the neutral geometry than the anion. The natures of the electron-accommodating orbitals in type I and the electron-releasing orbitals in type II are, of course, important for the geometrical effects. For example, electron removal from the $1b_{1g}$ and $2b_{3u}$ π orbitals in type II excitations favor the geometrical change in the same direction as the SOMO favors. On the other hand, the removal of an electron from the $4b_{3g}$ and $5b_{2u}$ n orbitals does not largely affect the geometry, though slight C═O bond shrinkage will be brought according to the electrostatic force theory.[32] (See the shapes of the corresponding MOs in Figure 1.) Therefore, the type II π−π*$_{SOMO}$ excitations result in larger energy increases than the n−π*$_{SOMO}$ excitations.

Assignments of the Experimentally Observed States. Table 9 shows the excitation energies of the *p*-BQ anion radical at its neutral geometry. The assignments given there are due to the experimentalists and the theoreticians who did the corresponding studies. The abbreviations of the experimental methods are given in the footnotes of Table 8.

The lowest excited state of the anion exists at about 0.7 eV above the neutral ground state at the neutral geometry. Our assignment of the lowest excited state is 1^2A_u (π_g^-*$_{SOMO}$−π_u^-* shape resonance) state, which is in accordance with the CASPT2 result by Pou-Amérigo et al.[17b] However, this assignment is different from those by other authors,[15a,16e,f] that is, $^2B_{3u}$. Except for Allan's, the assignments of $^2B_{3u}$ were based on the simple molecular orbital theory.[15a,16e] Because this system has relatively large electron correlations, such simple MO theory is rather dangerous. For example, the electron detachment from the n

TABLE 9: Comparison of Excitation Energies and Assignments by SAC−CI with Those by Experimental and Other Theoretical Results: Ground and Valence Excited States of the *p*-BQ Anion Radical at the Neutral Geometry[a]

experimental[b]				theoretical	
ETS[c] gas phase	ETS[d] gas phase	EELS[e] gas phase	SF_6SS[f] gas phase	SAC−CI[g]	CASPT2[h]
			Ground State ($^2B_{2g}$)		
			EA = 1.89[i]	EA = 1.57[j]	EA = 1.64[j]
			Excited States		
0.72	0.69 ($^2B_{3u}$)	0.77 ($^2B_{3u}$)	0.70 ($^2B_{3u}$)	0.83 (^2A_u [S])	0.91 (^2A_u [S])
				1.09 ($^2B_{3g}$ [F])	0.87 ($^2B_{3g}$ [F])
				1.22 ($^2B_{2u}$ [F])	0.96 ($^2B_{2u}$ [F])
1.43	1.41 (^2A_u)	1.6 (^2A_u)	1.35 (^2A_u)	1.79 ($^2B_{3u}$ [S])	1.31 ($^2B_{3u}$ [S])
2.15	2.11	2.0 ($^2B_{3u}$)	1.90 ($^2B_{3u}$)	2.44 ($^2B_{3u}$ [F])	1.87 ($^2B_{3u}$ [F + S])
				2.66 ($^2B_{1g}$ [F])	1.99 ($^2B_{1g}$ [F])

[a] [S] and [F] stand for shape and Feshbach resonances, respectively. All excitation energies are those from the neutral ground state. [b] See the footnotes of Table 8 for the abbreviations. [c] Reference 16d. [d] Reference 16e. The assignments were based on simple perturbation analysis of the MO energies. [e] Reference 16f. The assignments were based on analyses on the vibrational excitations in EELS. [f] Reference 15a. The assignments were based on PPP calculations. In ref 15a, these states were assigned to ^2A_u, $^2B_{3u}$, and $^2B_{2g}$, in the energy increasing order, but they revised the assignments afterward. [g] Present work. [h] Reference 17b. [i] Adiabatic electron affinity. [j] Vertical electron affinities.

orbital occurs more easily than that from the π orbital in contradiction with the orbital energy sequence.

On the other hand, Allan attributed the lowest three peaks in the constant-energy-loss EELS to the resonance states of the excited electron attached states and assigned them to $^2B_{3u}$, ^2A_u, and $^2B_{3u}$ in the light of the vibrational bands.[16f] The vibrational modes of the C=C and C=O stretch were enhanced in these excited states. These excited states experience the electron attachments to the C=C and C=O antibonding orbitals and/or the electron promotions from the C=C and C=O bonding orbitals. However, he did not state the order of these three excited states. We, rather, propose the following interpretation of his spectra; in his spectra (Figures 2 and 3 in ref 16f), the second and third electronic states favor the C=C and C=O stretch modes better than the C−H stretch mode, whereas the first one favors both. According to RRS results by Tripathi et al.[16a] and CASSCF vibrational analysis by Pou-Amérigo et al.,[17b] the $^2B_{3u}$ state will enhance the C=C and C=O stretching mode, and the ^2A_u state will enhance the ring breathing mode. The C−H stretch mixed with the C=C and C=O stretch forms the ring breathing mode, and this is consistent with the assignments that the lowest peak is ^2A_u and the second and the third are both $^2B_{3u}$.

The experimental excitation energies of higher states are similar and lie in the region of 1.3−1.6 and 1.9−2.2 eV above the neutral ground state. Thus, these experimental states can be assigned similarly. We assign the states at 1.3−1.6 and at 1.9−2.2 eV to 2^2B_{3u} and 3^2B_{3u}, respectively. The lower state is π_g^{-}*$_{SOMO}$−π_u^{+}* shape resonance state, and the higher one is π_u^{+}−π_g^{-}*$_{SOMO}$ Feshbach resonance state. These assignments are based on the excitation energies and the enhancements of the specific vibrational modes observed in EELS by Allan.[16f] The candidates for the third state at 1.9−2.2 eV were the Feshbach resonance 3^2B_{3u} and 2^2B_{1g} states. Although both states can enhance the C=C and C=O stretch, 3^2B_{3u} has much larger ability to enhance these mode, judging from their MO shapes, and therefore, we assigned the third state to 3^2B_{3u}. The calculated excitation energies for these states differ considerably from the experimental values, and we think that the reason is due to the mixing of the two-electron processes in these states, and this will be resolved by performing SAC−CI general-*R* calculations.[31]

Cooper et al. observed an excited anion state of *p*-BQ with an extremely long lifetime (>5 μs) at 1.40 eV above the detachment threshold besides the state at 1.35 eV in their SF_6SS.[15a] They explained the long lifetime in terms of intersystem crossing from this excited anion state to the ground state. Afterward, for this explanation, Schiedt et al. proposed a stepwise internal relaxation mechanism through a "ladder" of the two π−π*$_{SOMO}$ states rather than the direct one-step relaxation mechanism to the ground state.[15d] Our calculations can explain this long lifetime and support the interpretation of Schiedt et al. The excited state at 1.40 eV is assigned to the shape resonance $^2B_{3u}$ state according to the SAC−CI calculations. However, Figure 4 indicates that this state at the neutral geometry can switch the long-lived Feshbach state, $^2B_{3u}$, at the anion geometry. The electronic state can then compete with the ultrafast autodetachment processes and can undergo the internal relaxation with the dense ladder of the electronic states if the crossing is a conical intersection.

5.4. Diffuse Excited States of the *p*-BQ Anion Radical. Besides the valence excited states, several diffuse excited states were calculated in the energy region above the neutral ground state. The results using the anion geometry are summarized in Table 5, and those using the neutral geometry are summerized in Table 8. These states are described as the type I shape resonance states. Besides the calculations with the basis used previously (Basis1), we performed the calculations with extra basis functions, $n = 4$ Rydberg functions, in addition to the valence, polarization, anion diffuse, and $n = 3$ Rydberg basis functions (Basis2), at the anion geometry. The valence basis used in the Basis2 calculation was, however, double-ζ, whereas that in the Basis1 was triple-ζ.

The results for the Basis1 and Basis2 calculations are summarized in Table 10. The results for the Basis1 in Table 10 are the same one as those given in Table 5. The characters of the diffuse states for the anion molecule are different from that for the neutral molecule even if the state energies are lower than the electron detachment threshold, because the diffuse bound state for the anion is stabilized by the multipole of the neutral core molecule, whereas it is done by the Coulombic interaction with the cationic core for the case of the neutral molecule (Rydberg states). For the *p*-BQ anion, the diffuse state is thought to be a quadrupole-bound state. According to our SAC−CI results, the quadrupole moments of *p*-BQ were calculated to be −35, −30, and −52 au in the *xx*, *yy*, and *zz* directions, respectively. These are thought to be sufficiently large to form the quadrupole-bound states, and therefore, we believe that the diffuse bound states can exist below the electron detachment threshold. The energy of the 1^2A_g state becomes stable for the Basis2 calculation as compared to the Basis1 calculation, and this is expected to be a real state, not an artifact.

TABLE 10: Effects of Rydberg Basis Functions on Excited States of the *p*-BQ Anion Radical Calculated by SAC−CI at the Anion Geometry[a]

	Basis1[b]		Basis2[c]		
states	excitation energy [eV]	second moment [au]	excitation energy [eV]	second moment [au]	nature
$^2B_{2g}$	0.00	−139.7	0.00	−139.6	(anion ground state)
^2A_g	1.86	−295.0	1.70	−639.1	π_g^{-}*$_{SOMO}$−diff(s)
$^2B_{2u}$			1.85	−414.3	π_g^{-}*$_{SOMO}$−diff(p_y)
^2A_g			1.89	−716.0	π_g^{-}*$_{SOMO}$−diff($d_{x^2-y^2}$, d_{z^2})
$^2B_{3u}$			1.90	−415.2	π_g^{-}*$_{SOMO}$−diff(p_x)
$^2B_{1g}$			1.90	−709.5	π_g^{-}*$_{SOMO}$−diff(d_{xy})
$^2B_{3g}$			1.91	−724.9	π_g^{-}*$_{SOMO}$−diff(d_{yz})
^2A_g			1.92	−715.9	π_g^{-}*$_{SOMO}$−diff(d_{z^2}, $d_{x^2-y^2}$)
$^2B_{2g}$			1.92	−724.1	π_g^{-}*$_{SOMO}$−diff(d_{xz})
$^2B_{1u}$			1.95	−451.4	π_g^{-}*$_{SOMO}$−diff(p_z)
^2A_g			1.95	−668.3	π_g^{-}*$_{SOMO}$−diff(s)
^1A_g	EA = 1.96				(*neutral ground state*)
$^2B_{2u}$	2.28	−240.4	2.63	−319.9	π_g^{-}*$_{SOMO}$−diff(p_y)
$^2B_{3u}$	2.39	−226.4	2.72	−288.5	π_g^{-}*$_{SOMO}$−diff(p_x)
^2A_g	2.43	−306.2	2.44	−527.7	π_g^{-}*$_{SOMO}$−diff(s)
$^2B_{1u}$	2.48	−261.2	2.83	−318.4	π_g^{-}*$_{SOMO}$−diff(p_z), σ_u^{-}*
$^2B_{1g}$	2.50	−301.5	2.65	−357.8	π_g^{-}*$_{SOMO}$−diff(d_{xy})
$^2B_{3g}$	2.51	−321.4	2.66	−379.2	π_g^{-}*$_{SOMO}$−diff(d_{yz}), σ_g^{-}*
$^2B_{2g}$	2.57	−313.7	2.73	−365.4	π_g^{-}*$_{SOMO}$−diff(d_{xz})
^2A_g	2.59	−319.0	2.57	−359.4	π_g^{-}*$_{SOMO}$−diff(s), σ_g^{+}*
^2A_u	2.71	−141.3	2.72	−141.2	π_g^{-}*$_{SOMO}$−π_u^{-}*
^2A_g	2.77	−305.1	2.80	−385.2	π_g^{-}*$_{SOMO}$−diff(s), σ_g^{+}*
^2A_g			3.44	−398.8	π_g^{-}*$_{SOMO}$−diff(s), σ_g^{+}*
$^2B_{3u}$	3.74	−160.9	3.82	−160.8	π_g^{-}*$_{SOMO}$−π_u^{+}*
^2A_g	3.84	−231.9	3.98	−265.7	π_g^{-}*$_{SOMO}$−diff(s), σ_g^{+}*
$^2B_{3g}$	4.23	−251.3	4.38	−274.5	π_g^{-}*$_{SOMO}$−diff(d_{yz})
^2A_g	4.24	−261.9	4.68	−287.5	π_g^{-}*$_{SOMO}$−diff(s), σ_g^{+}*
$^2B_{1u}$	4.34	−225.5	4.35	−224.4	π_g^{-}*$_{SOMO}$−diff(p_z), σ_u^{-}*
$^2B_{2g}$	4.34	−236.8	4.48	−256.4	π_g^{-}*$_{SOMO}$−diff(d_{xz})
$^2B_{2u}$	4.40	−222.4	4.62	−205.8	π_g^{-}*$_{SOMO}$−diff(p_y), σ_u^{+}*
$^2B_{1g}$	4.44	−228.1	4.57	−246.4	π_g^{-}*$_{SOMO}$−diff(d_{xy})
$^2B_{3u}$	4.67	−194.4	5.01	−217.5	π_g^{-}*$_{SOMO}$−diff(p_x), π_u^{+}*

[a] Only Type I excitations were calculated. [b] Calculation with a basis set including $n = 3$ Rydberg basis functions. [c] Calculation with a basis set including $n = 3$ and 4 Rydberg basis functions. The valence basis functions for the Basis2 calculation were double-ζ, whereas those for the Basis1 calculation were triple-ζ.

The dramatic increase in the second moment may be attributed to a rather poor description of the diffuse character in the Basis1 calculation owing to the lack of the diffuse basis. For the Basis2 calculation, many diffuse states with much larger second moments were found at 1.7−2.0 eV above the anion ground state, and we assigned them to the diffuse bound (probably quadrupole-bound) states, because the energies are below the detachment threshold, 1.96 eV. It is inappropriate to call those states "Rydberg" states, because of the reason given above.

The non-Born−Oppenheimer (BO) effects would become important for very diffuse anion states. However, it was not treated in the present calculations because the non-BO effects that are due to the standard rotor constants of ca. 0.1 cm^{-1} are expected to be negligible in this case. This order of the rotor constants gives the upper limit of the mean radius of the surplus electron wave function in which the BO approximation is valid; it is 1000 au,[33] which is much larger than the radii for the calculated diffuse states.

On the other hand, the energy positions of most of the original diffuse states above the detachment threshold were not much affected by the enlargement of the basis set, except for the lowest diffuse p states. In other words, the addition of more diffuse functions resulted in just giving new diffuse bound states below the detachment threshold. They have the second moments larger by about 200 au than the higher diffuse states; that is, the higher diffuse states are spatially more compact. These states are thought to be the mixed valence-diffuse states and lie in the higher energy region than the detachment threshold as resonance states. However, to obtain more conclusive results, careful calculations with systematically enlarged diffuse bases would be necessary. The energy differences of the lowest diffuse p states between the Basis1 and Basis2 calculations are about 0.3 eV and would be attributed to the difference in the quality of the valence basis.

6. Summary

We calculated the ground, excited and ionized states of neutral *p*-BQ and the ground and excited states of its anion radical using the SAC/SAC−CI method. We assigned the peaks in the ionization spectra of *p*-BQ and the excited states of the *p*-BQ anion radical observed in various spectra.

The ionization peaks were assigned to be n_g^{-}, n_u^{+}, π_u^{+}, π_g^{+}, n_g^{-}, π_g^{-}, n_g^{+}, n_u^{-}, π_u^{+}, σ_u^{+}, σ_u^{-}, σ_g^{+}, σ_u^{+}, σ_g^{+}, and σ_g^{-} in energy increasing order. These peaks are mainly due to one-electron ionization processes, and the effect of the "shake-up" process to the spectra is small. For the anion radical, the calculations were performed at the equilibrium geometries for both the neutral and anion ground states. The adiabatic electron affinity and the excitation energies were calculated in good agreement with the experimental values. The first peak was assigned to the 1^2A_u (shape resonance π_g^{-}*$_{SOMO}$−π_u^{-}*) state in both geometries. We attributed the RRS assignments by Tripathi et al., that $^2B_{3u}$ is the lowest, as being due to the reverse ordering of the states because of the hydrogen bonds with water solvent, which was supported by the SAC−CI calculations for the *p*-BQH radical. In accordance with the proposal in the

literature, two forbidden n$-\pi^*_{SOMO}$ transitions were calculated below the lowest peak (^2A_u) for the anion geometry, whereas for the neutral geometry, these transitions were calculated to be higher than the ^2A_u state. Two higher allowed states in various spectra were assigned to $^2B_{3u}$ states ($\pi_u^+-\pi_g^-{}^*_{SOMO}$ and $\pi_g^-{}^*_{SOMO}-\pi_u^+{}^*$). The order, however, depended upon the geometries; that is, the $\pi_g^-{}^*_{SOMO}-\pi_u^+{}^*$ Feshbach resonance was lower at the anion geometry, and the $\pi_u^+-\pi_g^-{}^*_{SOMO}$ shape resonance was lower at the neutral geometry. The change in the ordering of the states is explained as being due to the change in the orbital energy caused by the change in geometry.

Acknowledgment. Part of this study has been supported by a Grant-in-Aid for Scientific Research from the Japanese Ministry of Education, Science, and Culture.

References and Notes

(1) Voet, D.; Voet, J. G. *Biochemistry*, 2nd ed.; John Wiley & Sons: New York, 1995; Chapter 22.

(2) (a) Nakatsuji, H.; Hasegawa, J.; Ohkawa, K. *Chem. Phys. Lett.* **1998**, *296*, 499. (b) Hasegawa, J.; Ohkawa, K.; Nakatsuji, H. *J. Phys. Chem. B* **1998**, *102*, 10410. (c) Hasegawa, J.; Nakatsuji, H. *J. Phys. Chem. B* **1998**, *102*, 10420. (d) Ito, H.; Nakatsuji, H. *J. Comput. Chem*. **2001**, *22*, 265. (e) Ohtsuka, Y.; Ohkawa, K.; Nakatsuji, H. *J. Comput. Chem*. **2001**, *22*, 521.

(3) Lown, J. W. *Chem. Soc. Rev.* **1993**, *22*, 165.

(4) Pryor, W. A.; Hales, B. J.; Premovic, P. I.; Church, D. F. *Science* **1983**, *220*, 425.

(5) Khodorkovsky, V.; Becker, J. Y. In *Organic Conductors*; Farges, J.-P., Ed.; Marcel Dekker: New York, 1994.

(6) (a) Eggins, B. R.; Chambers, J. Q. *J. Electrochem. Soc.* **1970**, *117*, 186. (b) Mitani, T.; Saito, G.; Urayama, H. *Phys. Rev. Lett.* **1988**, *60*, 2299.

(7) (a) Trommsdorff, H. P. *J. Chem. Phys.* **1972**, *56*, 5358. (b) Hollas, J. M. *Spectrochim. Acta* **1964**, *20*, 1563. (c) Brint, P.; Connerade, J.-P.; Tsekeris, P.; Bolovinos, A.; Baig, A. *J. Chem. Soc., Faraday Trans. 2* **1986**, *82*, 367. (d) Goodman, J.; Brus, L. E. *J. Chem. Phys.* **1978**, *69*, 1604.

(8) Meier, A. R.; Wagnière, G. H. *Chem. Phys.* **1987**, *113*, 287.

(9) Hochstrasser, R. M.; Johnson, L. W.; Trommsdorff, H. P. *Chem. Phys. Lett.* **1973**, *21*, 251.

(10) (a) Hug, W.; Kuhn, J.; Seibold, K.; Labhart, H.; Wagnière, G. *Helv. Chim. Acta* **1971**, *54*, 1451. (b) Stevenson, P. E. *J. Phys. Chem.* **1972**, *76*, 2424. (c) Merienne-Lafore, M. F.; Trommsdorff, H. P. *J. Chem. Phys.* **1976**, *64*, 3791.

(11) (a) Martin, R. L. *J. Chem. Phys.* **1981**, *74*, 1852. (b) Ha, T.-K. *Mol. Phys.* **1983**, *49*, 1471. (c) Pou-Amérigo, R.; Merchán, M.; Ortí, E. *J. Chem. Phys.* **1999**, *110*, 9536. (d) Weber, J.; Malsch, K.; Hohlneicher, G. *Chem. Phys.* **2001**, *264*, 275.

(12) (a) Brundle, C. R.; Robin, M. B.; Kuebler, N. A. *J. Am. Chem. Soc.* **1972**, *94*, 1466. (b) Åsbrink, L.; Bieri, G.; Fridh, C.; Lindholm, E.; Chong, D. P. *Chem. Phys.* **1979**, *43*, 189. (c) Dougherty, D.; McGlynn, S. P. *J. Am. Chem. Soc.* **1977**, *99*, 3234. (d) Stanton, J. F.; Sattelmeyer, K. W.; Gauss, J.; Allan, M.; Skalicky, T.; Bally, T. *J. Chem. Phys.* **2001**, *115*, 1.

(13) (a) Stanton, J. F.; Gauss, J. *J. Chem. Phys.* **1994**, *101*, 8938. (b) Christiansen, O.; Koch, H.; Jørgensen, P. *Chem. Phys. Lett.* **1995**, *243*, 409.

(14) (a) Jonkman, H. T.; van der Velde, G. A.; Nieuwpoort, W. C. In *Quantum Chemistry, The state of the art, Proceedings of S. R. C.*; Atlas Symposium No. 4; 1974; p 243. (b) Wood, M. H. *Theor. Chim. Acta* **1975**, *36*, 345. (c) Bigelow, R. W. *J. Chem. Phys.* **1978**, *68*, 5086.

(15) (a) Cooper, C. D.; Naff, W. T.; Compton, R. N. *J. Chem. Phys.* **1975**, *63*, 2752. (b) Marks, J.; Comita, P. B.; Brauman, J. I. *J. Am. Chem. Soc.* **1985**, *107*, 3718. (c) Comita, P. B.; Brauman, J. I. *J. Am. Chem. Soc.* **1987**, *109*, 7591. (d) Schiedt, J.; Weinkauf, R. *J. Chem. Phys.* **1999**, *110*, 304.

(16) (a) Tripathi, G. N. R.; Sun, Q.; Schuler, R. H. *Chem. Phys. Lett.* **1989**, *156*, 51. (b) Shida, T. In *Physical Sciences Data 34 "Electronic absorption spectra of radical ions"*; Elsevier: Amsterdam, The Netherlands, 1988; p 308. (c) Cook, A. R.; Curtiss, L. A.; Miller, J. R. *J. Am. Chem. Soc.* **1997**, *119*, 5729. (d) Allan, A. *Chem. Phys.* **1983**, *81*, 235. (e) Modelli, A.; Burrow, P. D. *J. Phys. Chem.* **1984**, *88*, 3550. (f) Allan, A. *Chem. Phys.* **1984**, *84*, 311.

(17) (a) Wheeler, R. A. *J. Phys. Chem.* **1993**, *97*, 1533. (b) Pou-Amérigo, R.; Serrano-Andrés, L.; Merchán, M.; Ortí, E.; Forsberg, N. *J. Am. Chem. Soc.* **2000**, *122*, 6067.

(18) Nakatsuji, H.; Hirao, K. *J. Chem. Phys.* **1978**, *68*, 2053.

(19) (a) Nakatsuji, H. *Chem. Phys. Lett.* **1978**, *59*, 362. (b) Nakatsuji, H. *Chem. Phys. Lett.* **1979**, *67*, 329, 334.

(20) (a) Nakatsuji, H. *Acta Chim. Hung.* **1992**, *129*, 719. (b) Nakatsuji, H. In *Computational Chemistry, Reviews of Current Trends*; Leszczynski, J., Ed.; World Scientific: Singapore, 1997; Vol. 2.

(21) Dunning, T. H., Jr. *J. Chem. Phys.* **1970**, *53*, 2823.

(22) Huzinaga, S.; Andzelm, J.; Klobukowski, M.; Radzio-Andzelm, E.; Sakai, Y.; Tatewaki, H. *Gaussian Basis Set for Molecular Calculations*; Elsevier: Amsterdam, 1984.

(23) Dunning, T. H., Jr.; Hay, P. J. In *Modern Theoretical Chemistry*; Schaefer, H. F., III., Ed.; Plenum: New York, 1977; Vol. 3, p 1.

(24) Hagen, K.; Hedberg, K. *J. Chem. Phys.* **1973**, *59*, 158.

(25) (a) Nakatsuji, H. *Chem. Phys.* **1983**, *75*, 425. (b) Nakatsuji, H.; Hasegawa, J.; Hada, M. *J. Chem. Phys.* **1996**, *104*, 2321. (c) Tokita, Y.; Hasegawa, J.; Nakatsuji, H. *J. Phys. Chem. A* **1998**, *102*, 1843.

(26) Nakatsuji, H.; Hada, M.; Ehara, M.; Hasegawa, J.; Nakajima, T.; Nakai, H.; Kitao, O.; Toyota, K. SAC/SAC−CI program system (SAC−CI96) for calculating ground, excited, ionized, and electron attached states and singlet to septet spin multiplicities, 1998.

(27) Frisch, M. J.; Trucks, G. W.; Schlegel, H. B.; Scuseria, G. E.; Robb, M. A.; Cheeseman, J. R.; Zakrzewski, V. G.; Montgomery, J. A.; Stratmann, R. E.; Burant, J. C.; Dapprich, S.; Millam, J. M.; Daniels, A. D.; Kudin, K. N.; Strain, M. C.; Farkas, O.; Tomasi, J.; Barone, V.; Cossi, M.; Cammi, R.; Mennucci, B.; Pomelli, C.; Adamo, C.; Clifford, S.; Ochterski, J.; Petersson, G. A.; Ayala, P. Y.; Cui, Q.; Morokuma, K.; Malick, D. K.; Rabuck, A. D.; Raghavachari, K.; Foresman, J. B.; Cioslowski, J.; Ortiz, J. V.; Stefanov, B. B.; Liu, G.; Liashenko, A.; Piskorz, P.; Komaromi, I.; Gomperts, R.; Martin, R. L.; Fox, D. J.; Keith, T.; Al-Laham, M. A.; Peng, C. Y.; Nanayakkara, A.; Gonzalez, C.; Challacombe, M.; Gill, P. M. W.; Johnson, B. G.; Chen, W.; Wong, M. W.; Andres, J. L.; Head-Gordon, M.; Replogle, E. S.; Pople, J. A. *Gaussian 98*, revision A.1; Gaussian Inc.: Pittsburgh, PA, 1998.

(28) Martin, R. L.; Shirley, D. A. *J. Chem. Phys.* **1976**, *64*, 3685.

(29) (a) Åsbrink, L.; Fridh, C.; Lindholm, E.; de Bruijn, S. *Chem. Phys. Lett.* **1979**, *66*, 411. (b) de Bruijn, S. *Chem. Phys. Lett.* **1977**, *52*, 76. (c) de Bruijn, S. *Theor. Chim. Acta* **1979**, *50*, 313.

(30) Köppel, H.; Domcke, W.; Cederbaum, L. S. *Adv. Chem. Phys.* **1984**, *57*, 59.

(31) Nakatsuji, H. *Chem. Phys. Lett.* **1991**, *177*, 331.

(32) See, e.g.: Nakatsuji, H. *J. Am. Chem. Soc.* **1973**, *95*, 345, 354, 2084. Nakatsuji, H.; Koga, T. In *The Force Concept in Chemistry*; Deb, B. M., Ed.; Van Nostrand Reinhold: New York, 1981; Chapter 3.

(33) Abdoul-Carime, H.; Desfrançois, C. *Eur. Phys. J. D* **1998**, *2*, 149.